PROCEEDINGS OF SPIE

SPIEDigitalLibrary.org/conference-proceedings-of-spie

Assessment of DBT acquisition parameters for 2D and 3D search tasks

Howard C. Gifford, Mini Das

Howard C. Gifford, Mini Das, "Assessment of DBT acquisition parameters for 2D and 3D search tasks," Proc. SPIE 10577, Medical Imaging 2018: Image Perception, Observer Performance, and Technology Assessment, 105770I (7 March 2018); doi: 10.1117/12.2294984



Event: SPIE Medical Imaging, 2018, Houston, Texas, United States

Assessment of DBT acquisition parameters for 2D and 3D search tasks

Howard C. Gifford¹ and Mini Das^{1,2}

¹Department of Biomedical Engineering; ²Department of Physics University of Houston, Houston, TX

ABSTRACT

A concern with using mathematical model observers to gauge medical image quality is whether and to what degree task simplifications can affect study outcomes. Researchers are interested in assessments based on clinically realistic tasks, but routinely implement simplified tasks to manage time and computation. The goal of this work is to examine how optimization of digital breast tomosynthesis (DBT) acquisition parameters can be influenced by the consideration of 2D or 3D search tasks. Localization ROC (LROC) observer studies were based on simulated image slices and volumes obtained from low- and medium-density digital breast phantoms containing 8-mm spherical masses. An analytic cone-beam projector used an acquisition arc of 60° while the number of angular projections varied from 3 to 51. Image volumes were reconstructed with the Feldkamp FBP algorithm and then postfiltered and thresholded to eliminate negative pixel values. A visual-search (VS) model observer was applied for both the 2D and 3D LROC studies. The observer used 2D spatial derivatives as features to find suspicious candidate locations in an image. The candidates were compared by means of a binary Hotelling discriminant. Preliminary results indicated substantially reduced performance with the 3D task, particularly for the more-dense cases.

1. INTRODUCTION

As a form of limited-angle 3D tomography, DBT can provide reduced anatomical noise compared to mammograms. However, DBT currently functions primarily as an adjunct for mammography, offering improved mass detection while often degrading microcalcification detection. Researchers working to optimize DBT operational parameters frequently make use of clinically relevant task-based metrics.

A number of studies^{1–5} have used model observers to investigate how acquisition geometry (number of projections and angular range) affects the image quality of DBT systems. Some of these studies have involved target search and some have dealt with image volumes, but relatively few have considered 3D search with breast volumes. A frequent concern with model observer studies in general is how task simplification can affect study outcomes. Thus, our objective is to examine how the optimization of a DBT acquisition protocol can be influenced by the use of 2D or 3D search tasks. The work is being carried out with VS observers, which have shown good correlation with human observers for a variety of x-ray and nuclear medicine applications.^{6–9}

The initial results presented herein are from localization receiver operating characteristic (LROC) studies of mass detection with a single VS observer. The VS observer identified suspicious locations in an image as local maxima in a set of feature maps and then applied a binary linear discriminant that was constructed from candidate feature statistics accrued through training. VS observers have been previously compared against humans with 2D DBT images, but the linear discriminant is new to this work. The observer applied for the DBT volumes extended a 3D VS observer model that was used previously for SPECT.

Further author information: E-mail: hgifford@uh.edu

Medical Imaging 2018: Image Perception, Observer Performance, and Technology Assessment, edited by Robert M. Nishikawa, Frank W. Samuelson, Proc. of SPIE Vol. 10577, 105770I
© 2018 SPIE · CCC code: 1605-7422/18/\$18 · doi: 10.1117/12.2294984

2. METHODS

2.1 Breast Phantoms

Multiple compressed-breast digital backgrounds were generated from one geometry of the Bakic phantom.¹⁰ The dimensions of the phantoms were $1020 \times 323 \times 257$, with a voxel width of 0.2 mm. We defined low and medium-density breasts based on mean percent densities of 25% and 50%, respectively. Three background realizations were generated for each density.

Eight single-mass cases were created from each background, giving a total of 27 cases (24 lesion-present and 3 lesion-absent) per density. The masses were homogeneous spheres with a diameter of 8.0 mm. These spheres were randomly placed in the fibroglandular compartment of the breast. The relative contrast of the masses was only a few percent. Example slices from the phantoms are shown in Fig. 1.

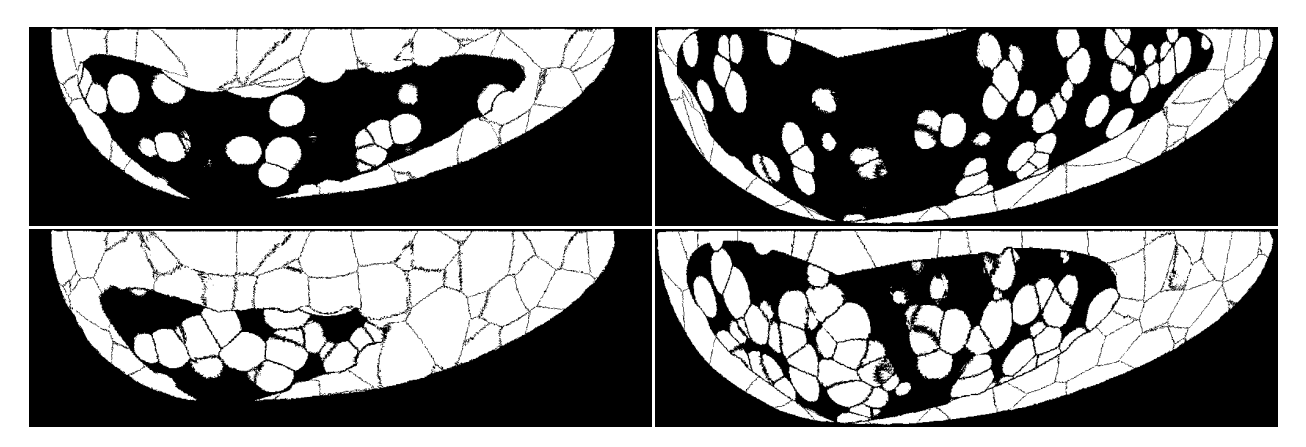


Figure 1. Sample slices from (top) the medium-density and (bottom) low-density Bakic phantoms. The overall breast volume is the same for both phantoms. The solid black area within each breast represents the fibroglandular compartment. The white areas are adipose tissue.

2.2 DBT Simulation

Our DBT imaging model has been described previously.⁶ X-ray transmissions with a rotating source-detector geometry and step-and-shoot protocol are generated by ray tracing.¹¹ A serial cascade model is used for the subsequent propagation of signals and noise through a CsI-based amorphous silicon flat-panel detector. The imaging model accounts for both focal-spot blur and scintillator blur. The dependence of scintillator blur on angle of incidence was not included and scatter also was not modeled. The imaging assumed a filtered molybdenum spectra at 30 kVp and a detector pixel size of 100 μ m. In this work, the angular acquisition arc was fixed at 60 degrees and the number of projections ranged from 3 to 51. Each acquisition was constrained to a 2.0-mGy average glandular dose.

2.3 Synthetic Images

3D DBT reconstructions applied the Feldkamp filtered backprojection algorithm. The voxel dimensions of the reconstruction were $760 \times 240 \times 195$ and the voxel width was 0.27 mm. Postreconstruction smoothing was carried out with a fifth-order 3D Butterworth filter having a cutoff frequency of 0.25 pixel⁻¹. Five-slice slabbing was then applied in the z dimension and negative pixel values in the slabbed volumes were truncated to zero. Figure 2 compares sample postfiltered slices and corresponding slabbed/thresholded slices that were obtained for both phantom densities and different numbers of projection angles.

The 3D observer study used the volume reconstructions from the 54 cases (48 lesion-present and 6 lesion-absent) described in Sec. 2.2. For the 2D study, a single slice was extracted from each of the lesion-present volumes and 8 slices were extracted from each lesion-absent volume, giving a total of 96 2D cases equally split between normal and abnormal cases. Each lesion-present slice contained the center coordinates of the mass.

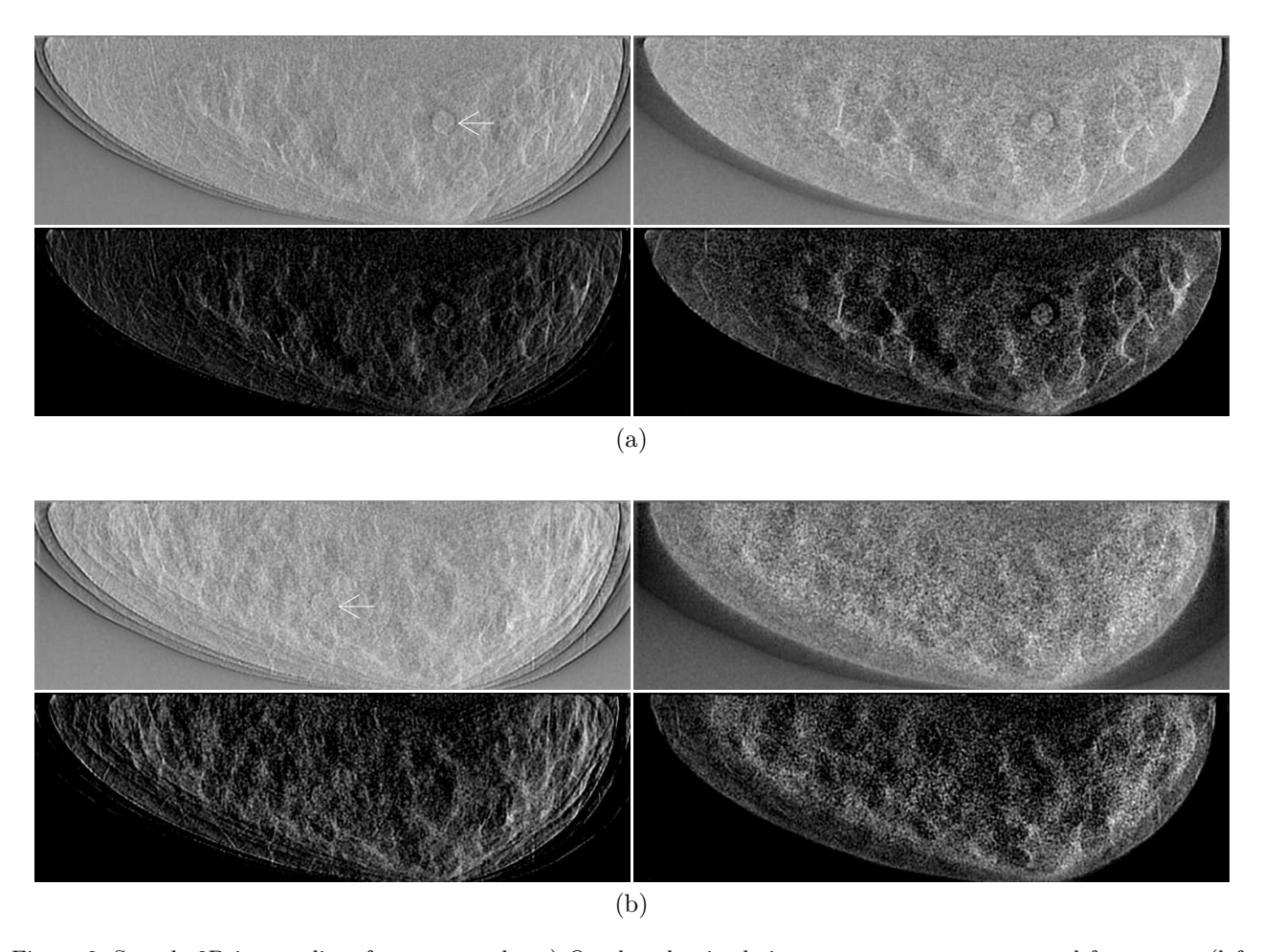


Figure 2. Sample 2D image slices from our study. a) One low-density lesion-present case reconstructed from seven (left column) and 45 (right column) projection angles. Images in the top row only have Butterworth filtering while those in the bottom row were also slabbed and thresholded. b) A medium-density case with lesion is shown using the same numbers of angles as in (a). The lesion positions are indicated by the arrows.

2.4 The 2D VS Observer

For a 2D test image f, the VS observer computed three matched-filter type feature maps of the form

$$\mathbf{p}_{\mathcal{O}} = \mathcal{O}\{\mathbf{s}\} \star \star \mathcal{O}\{\mathbf{f}\},\tag{1}$$

with **s** as the mean 2D lesion profile in the study, operator \mathcal{O} as a spatial derivative, and '*** denoting 2D correlation. The observer used the 2D gradient $(\frac{\partial}{\partial x}, \frac{\partial}{\partial y})$ as well as the separate horizontal and vertical derivatives $(\frac{\partial}{\partial x} \text{ and } \frac{\partial}{\partial y}, \text{ respectively})$ as the operators in Eq. 1. The correlation kernels obtained by applying the separate derivatives to **s** are shown in Fig. 3. Watershed segmentation was conducted on each map to identify local maxima within the fibroglandular region as candidate locations. A binary Hotelling discriminant computed from the candidate feature statistics was then applied to determine the most suspicious location and the LROC confidence rating.

In the 2D study, the 96 test images were used for both training and testing. The training involved estimation of the mean reconstructed lesion profile and calculation of the discriminant. The LROC data was analyzed with a 14.0-pixel radius of correct localization, approximately equal to the radius of the reconstructed lesion. Larger radii (up to 25 pixels) did not substantially change our results. The fraction of lesions correctly localized was used as the performance figure of merit.

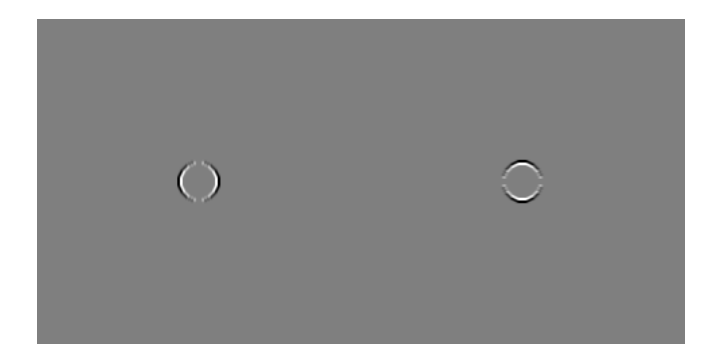


Figure 3. The correlation kernels obtained by applying the spatial derivatives (left) $\frac{\partial}{\partial x}$ and (right) $\frac{\partial}{\partial y}$ to the mean 2D reconstructed lesion profile. These kernels were used in Eq. 1 to generate the three feature maps for the 2D and 3D VS observers.

2.5 The 3D VS Observer

For our 3D model observer, Eq. 1 was replaced with a 3D cross-correlation involving image volume ${\bf f}$ and the mean reconstructed lesion ${\bf s}$. However, the same three spatial derivative operators as in the 2D study were applied on a slice-by-slice basis to ${\bf s}$ and ${\bf f}$. A 3D watershed algorithm was applied to determine candidate locations. The feature extraction thus integrated over five slices — approximately the slabbed diameter of the lesion — throughout the DBT volume.

As was the case with the 2D study, all of the available image volumes were used for both the training and testing phases of the 3D study. The localization radius also matched that of the 2D study.

3. RESULTS

The plots in Fig. 4 show how observer performance in the 2D study varied with the number of projections and the phantom density. These results are quite similar to those obtained in an earlier DBT study that used Butterworth-filtered slices without slabbing or truncation.⁶ That prior study included validation against human observers.

The data acquisition for the 3D study is ongoing, as is verification of the observer results. Figure 5 presents a sample of the available data., showing observer performance as a function of phantom density for the 2D and 3D images reconstructed from 15 projection angles. Performance decreased considerably with the image volumes, particularly with the medium-density cases.

4. CONCLUSIONS

We have presented initial results from a comparison of 2D and 3D detection-localization studies with a VS model observer. The 2D results are similar to those from a previous study. Work is ongoing to validate the 3D observer and improve the computational efficiency. Future work will include 2D and 3D location-known studies as part of a same-observer task comparison. We shall also investigate different feature sets. Both masses and microcalcifications will be treated in our studies.

REFERENCES

- 1. A. S. Chawla, J. Y. Lo, J. A. Baker, and E. Samei, "Optimized image acquisition for breast tomosynthesis in projection and reconstruction space.," *Medical Physics*, vol. 36, pp. 4859–4869, Nov. 2009.
- 2. S. Park, R. J. Jennings, H. Liu, A. Badano, and K. J. Myers, "A statistical, task-based evaluation method for three-dimensional x-ray breast imaging systems using variable-background phantoms.," *Medical Physics*, vol. 37, pp. 6253–6270, Dec. 2010.

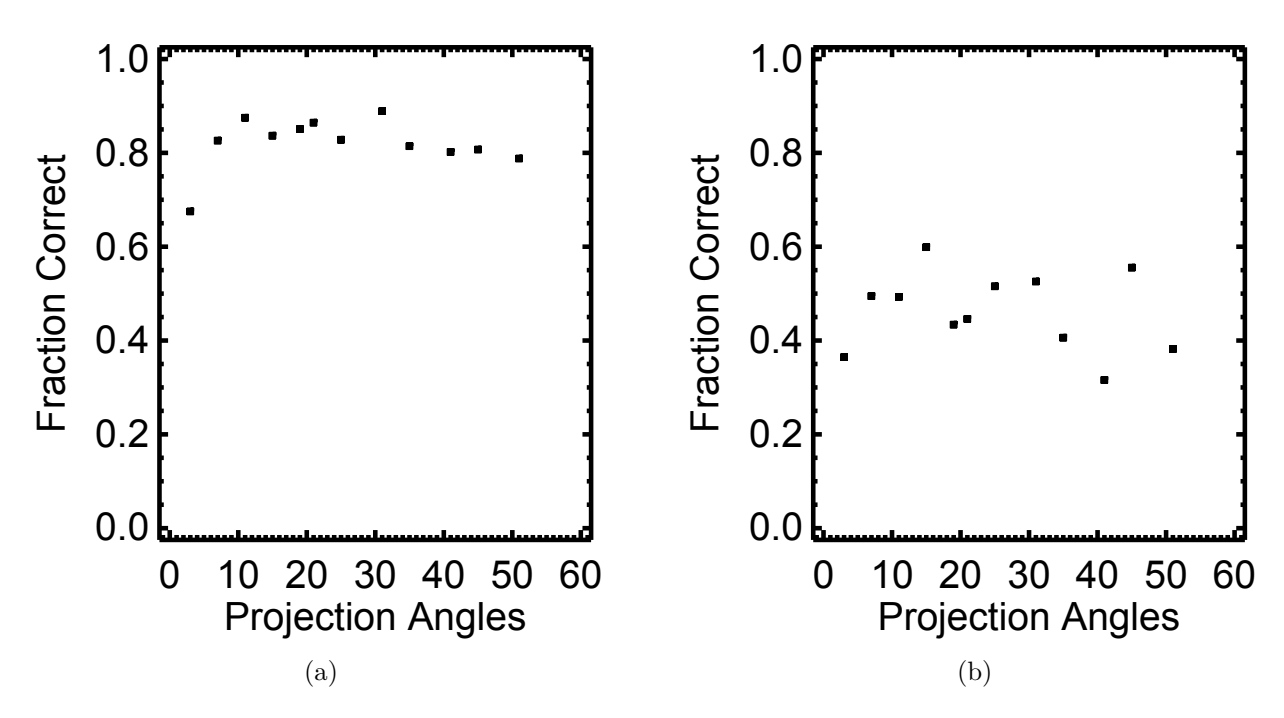


Figure 4. Observer performance with 2D images as a function of the number of projection angles for images generated from a) the low-density and b) medium-density phantoms.

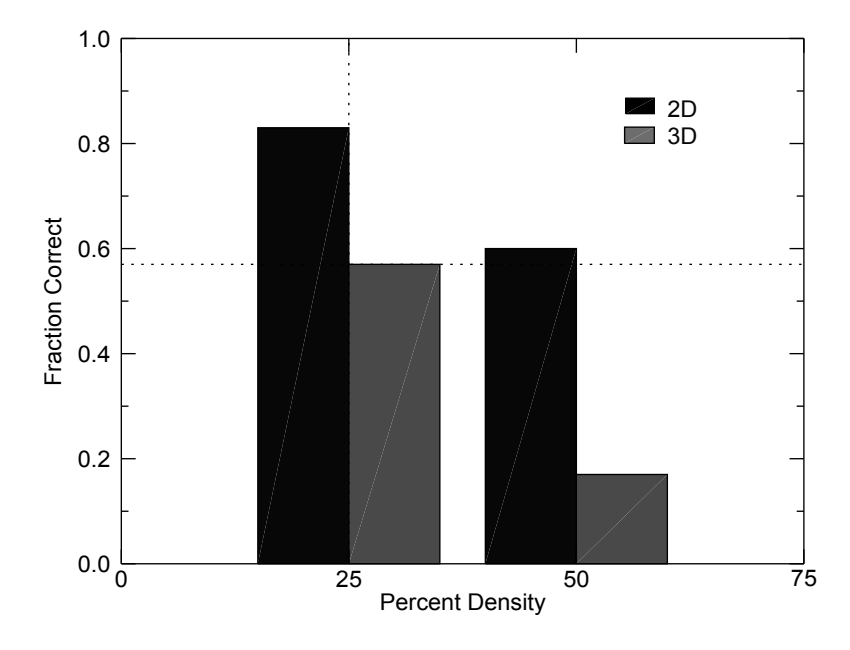


Figure 5. Observer performance with 2D and 3D images as a function of phantom density when 15 projection angles were used for the reconstruction.

- 3. I. S. Reiser and R. M. Nishikawa, "Task-based assessment of breast tomosynthesis: effect of acquisition parameters and quantum noise," *Medical Physics*, vol. 37, pp. 1591–1600, Mar. 2010.
- 4. B. A. Lau, M. Das, and H. C. Gifford, "Towards Visual-Search Model Observers for Mass Detection in

- Breast Tomosynthesis," *Proceedings of SPIE*, vol. 8668, p. 86680X, Mar. 2013.
- R. Zeng, S. Park, P. R. Bakic, and K. J. Myers, "Evaluating the sensitivity of the optimization of acquisition geometry to the choice of reconstruction algorithm in digital breast tomosynthesis through a simulation study.," *Physics in Medicine and Biology*, vol. 60, pp. 1259–1288, Feb. 2015.
- 6. H. C. Gifford, Z. Liang, and M. Das, "Visual-search observers for assessing tomographic x-ray image quality.," *Medical Physics*, vol. 43, pp. 1563–1575, Mar. 2016.
- H. C. Gifford, "Efficient Visual-Search Model Observers for PET," British Journal of Radiology, vol. 87, p. 20140017, May 2014.
- 8. H. C. Gifford, "A visual-search model observer for multislice-multiview SPECT images," *Medical Physics*, vol. 40, p. 092505, Sept. 2013.
- 9. Z. Karbaschi and H. C. Gifford, "Visual-Search Model Observer for Assessing Mass Detection in CT," *Proceedings of SPIE*, vol. 10136, p. 1013613, Mar. 2017.
- 10. P. R. Bakic, M. Albert, D. Brzakovic, and A. D. A. Maidment, "Mammogram synthesis using a 3D simulation. I. Breast tissue model and image acquisition simulation.," *Medical Physics*, vol. 29, pp. 2131–2139, Sept. 2002.
- 11. X. Gong, S. J. Glick, B. Liu, A. A. Vedula, and S. Thacker, "A computer simulation study comparing lesion detection accuracy with digital mammography, breast tomosynthesis, and cone-beam CT breast imaging," *Medical Physics*, vol. 33, pp. 1041–1052, Apr. 2006.
- 12. L. A. Feldkamp, L. C. Davis, and J. W. Kress, "Practical Cone-Beam Algorithm," *Journal of the Optical Society of America A*, vol. 1, no. 6, pp. 612–619, 1984.
- 13. R. Fiete and H. H. Barrett, "Using the Hotelling trace criterion for feature enhancement in image processing," *Optics Letters*, vol. 12, no. 9, pp. 643–645, 1987.